Philosophical Magazine A
Publication details, including instructions for authors and subscription information:
http://www.tandfonline.com/loi/tpha20

Twinning in $AuCu_3(Ag)$ II long-period superlattice

I. Goldfarb [a] , E. Zolotoyabko [b] & M. Bamberger [b]
[a] Department of Materials, Oxford University, Oxford, OX1 3PH, UK
[b] Department of Materials Engineering, Technion-Israel Institute of Technology, Haifa, 32000, Israel
Version of record first published: 27 Sep 2006.

To cite this article: I. Goldfarb , E. Zolotoyabko & M. Bamberger (1995): Twinning in $AuCu_3(Ag)$ II long-period superlattice, Philosophical Magazine A, 72:4, 981-996

To link to this article: http://dx.doi.org/10.1080/01418619508239948

PHILOSOPHICAL MAGAZINE A, 1995, VOL. 72, NO. 4, 981–996

Twinning in $AuCu_3$(Ag) II long-period superlattice

By I. GOLDFARB

Department of Materials, Oxford University, Oxford OX1 3PH, UK

E. ZOLOTOYABKO and M. BAMBERGER

Department of Materials Engineering, Technion–Israel Institute of Technology, Haifa 32000, Israel

[*Received 10 October 1994*† *and accepted 1 May 1995*]

ABSTRACT

Ternary Au–Ag–Cu alloys differing in composition were produced by means of a sequential gradual sputtering of elemental thin films. The resultant multilayers were then subjected to various heat treatments to promote a phase formation by interdiffusion. A long-period superlattice $AuCu_3$ II was found among the different phases. The microstructure of this phase revealed growth stacking faults and twins. The defect formation is explained by a semi-quantitative model based on the electron theory of metals. Some applications of this model concerning the domain size of long-period superlattices are also discussed.

§ 1. INTRODUCTION

Long-period superlattices (LPSs) in the Au–Cu system have attracted considerable attention in the past few decades (Pashley and Presland 1959, Sato and Toth 1963, Ogawa 1974, Takeda and Hashimoto 1985). There are two LPSs in the Au–Cu system, namely: AuCu II based on the $L1_0$ subcell and $AuCu_3$ II based on the $L1_2$ subcell. The location of these phases in equilibrium diagrams as well as their crystallography have been described in several works (Sato and Toth 1963, Barret and Massalski 1980). There are numerous studies analysing the properties and especially the stability of these LPS, as well as LPS in other systems, and among them an important contribution to the LPS theory was made by Sato and Toth (Sato and Toth 1961, 1962, Toth and Sato 1962). Their model, based on the original ideas of Jones (1934 a, b, 1937), assumes stability of LPSs taking into consideration electronic states in the periodic lattice potential and the resultant contact between the Fermi surface and the Brillouin zone boundaries. Following Sato and Toth, the periodic displacement of atoms (i.e. LPS formation) fosters energy lowering of the conduction electrons. Their model also predicts the domain size (M) as a function of e/a, which is in excellent agreement with experimental data. The validity of their model was further shown by recent work (Gyorffy and Stocks 1983, Stocks *et al.* 1987), which put it on more solid ground, using modern quantitative calculations. However, Sato and Toth's model in its original form, does not provide any thermodynamical treatment of the problem. It was suggested (Takeda, Kulik and de Fontaine 1987) that there are two kinds of LPS: those with sharp periodic antiphase boundaries (PAPBs), such as Al_3Ti and Ag_3Mg, and those exhibiting more diffuse behaviour of PAPBs, such as Au–Cu and Cu_3Pd (the distinction between the two is not

† Received in final form 26 February 1995.

straightforward). The axial next nearest neighbour Ising (ANNNI) model can be applied to the former LPS while the latter are regarded as 'Fermi surface driven'. On the other hand, recent work (Jordan *et al.* 1993) provides evidence that the Fermi surface topology serves as a driving force even for the Ag–Mg alloys. Therefore, it may be alternatively stated that the interaction of the Fermi surface with the superlattice Brillouin zone boundaries is the reason for long-range interactions in the alloy, which can be treated in the framework of statistical thermodynamics using the ANNNI model (Takeda *et al.* 1987).

Microstructural analysis has been performed by many investigators (Glossop and Pashley 1959, Marcinkowski and Zwell 1963, Yasuda 1987, Nakagawa and Yasuda 1988). The characteristic image of LPS consists of unidirectional zones, with PAPBs forming at right angles to one another. This is not surprising, since antiphase boundaries (APBs) form on the {001} atomic planes, as a result of the lower APB energy on them (Flinn 1958, Sato and Toth 1962). To the best of our knowledge, twins have never been detected in $AuCu_3$ II until recently by the authors (Goldfarb, Zolotoyabko and Shechtman 1993a). These twins studied by transmission electron microscopy (TEM), show unusual angles between the unidirectional zones, which differ considerably from a right angle. Selected area electron diffraction (SAED) and careful trace analysis have proved the existence of coherent twins related to the matrix by Kelly's relations (Kelly 1965). There are also stacking faults (SFs), which are most probably embryonic twins, i.e. part of these SFs transform into twins during the growth process (Shechtman, Blackburn and Lipsitt 1974). Some kind of faulting lying in the plane of PAPBs in AuCu II has been detected by Takeda and Hashimoto using high-resolution electron microscopy (Takeda and Hashimoto 1985).

Generally, twins are not to be expected in highly ordered alloys, since such a faulting destroys the order (Flinn 1958). However, in some cases faulting might be favourable, taking into account an electronic contribution to the free energy of the system, as was pointed out by Mikkola and Cohen (1961). More recent calculations of fault energies in $L1_2$-type structures show various degrees of stability as a function of fault character, such as superlattice intrinsic stacking fault (SISF), complex stacking fault (CSF), APB or superlattice extrinsic stacking fault (SESF) (Yamaguchi, Vitek and Pope 1981, Paxton 1992).

In this article we present TEM images together with SAED patterns giving evidence of growth twin formation in $AuCu_3$ II LPS. An attempt is made to explain the observed twinning in the framework of the electron energy gain, following the interaction of a Fermi surface with a diffused hexagonal Brillouin zone, locally formed by SISF (Mikkola and Cohen 1961).

§ 2. Experimental procedures

Samples were prepared by subsequent magnetron d.c. plasma sputtering from 3 in 99·99% Au, Ag and Cu elemental targets, using high-purity Ar. Prior to deposition the sputtering chamber was evacuated to $1{\cdot}3 \times 10^{-5}$ Pa, and then, after 30 min of presputtering, deposition took place onto 55 Formvar-coated EM Mo grids with a dynamic pressure of 0·4 Pa. Using a substrate shutter especially developed for this purpose, we have obtained as set of 55 differently composed Au–Ag–Cu samples with a uniform thickness of about 3500 Å. Each sample was composed of 90 wedge-shaped alternating Au, Ag and Cu thin multilayers with gradually varied thicknesses. These untreated samples were analysed by X-ray diffraction (XRD) and by energy dispersive spectroscopy (EDS). The measurements demonstrated the formation of artificially

composition-modulated superstructures with a superperiod of $H = 120$ Å and fluctuations of $\Delta H/H = 1{\cdot}5\%$. Details of the sample preparation and the preliminary characterizations were given previously (Goldfarb *et al.* 1993b, Goldfarb, Zolotoyabko, Berner and Shechtman 1994).

All samples were heat-treated in a $1{\cdot}3 \times 10^{-4}$ Pa dynamic vacuum furnace. The relevant samples were homogenized at 500–550°C for 3–6 h, and then treated at the ordering temperatures of 300–350°C for 6–17 h. Such annealing periods are quite sufficient for homogenization and ordering, as shown by Menon *et al.* (1992) and confirmed by our XRD and TEM data (Goldfarb *et al.* 1993 a, b, 1994).

§ 3. Results

XRD spectra of the heat-treated samples were measured in Bragg–Brentano parafocusing geometry using a conventional X-ray powder diffractometer, equipped with bent graphite monochromator and Cu radiation tube. Each scan was performed in a step mode with step size $\Delta 2\Theta = 0{\cdot}035°$ and 10 s of exposure per step. These spectra (presented in our other work (Goldfarb *et al.* 1994)) revealed phase formation in general accordance with the equilibrium Au–Ag–Cu phase diagram (Prince 1988).

Microstructural studies were conducted using a 200 kV scanning transmission electron microscope equipped with EDS adequate for thin-film microanalysis. Prior to introduction into the scanning transmission electron microscope column, the samples were thinned using an ion-miller, using a plasma voltage of 4 kV and a 16° beam inclination. A typical microstructure of the $\alpha_1 + AuCu_3$-containing samples is shown in fig. 1. The results to be discussed in this article were obtained by sampling a large number of grains by SAED, EDS and digital X-ray mapping (DXM). Therefore, they represent the general features of the phase formed.

Figure 1 presents two distinct kinds of grain, designated 1 and 2. Type-1 grains exhibit large parallel-sided twin-bands contrast. The SAED pattern from such a grain is characteristic of a $\{111\}\langle 112\rangle$ f.c.c. twin. This pattern together with its computer simulation for α_1 is shown in fig. 2 (*a*). The dark-field (DF) image using twin reflections is shown in fig. 2 (*b*). Thus, type-1 grains are representative of the $\alpha_1$phase.

Fig. 1

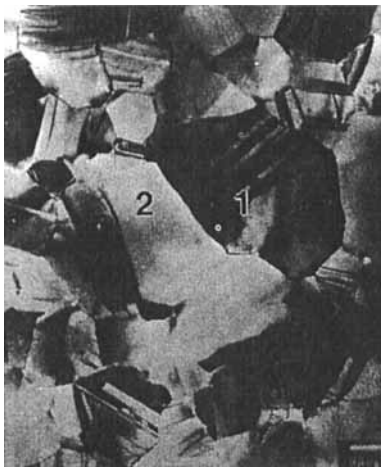

Typical microstructure of the $\alpha_1 + AuCu_3$ samples.

Fig. 2

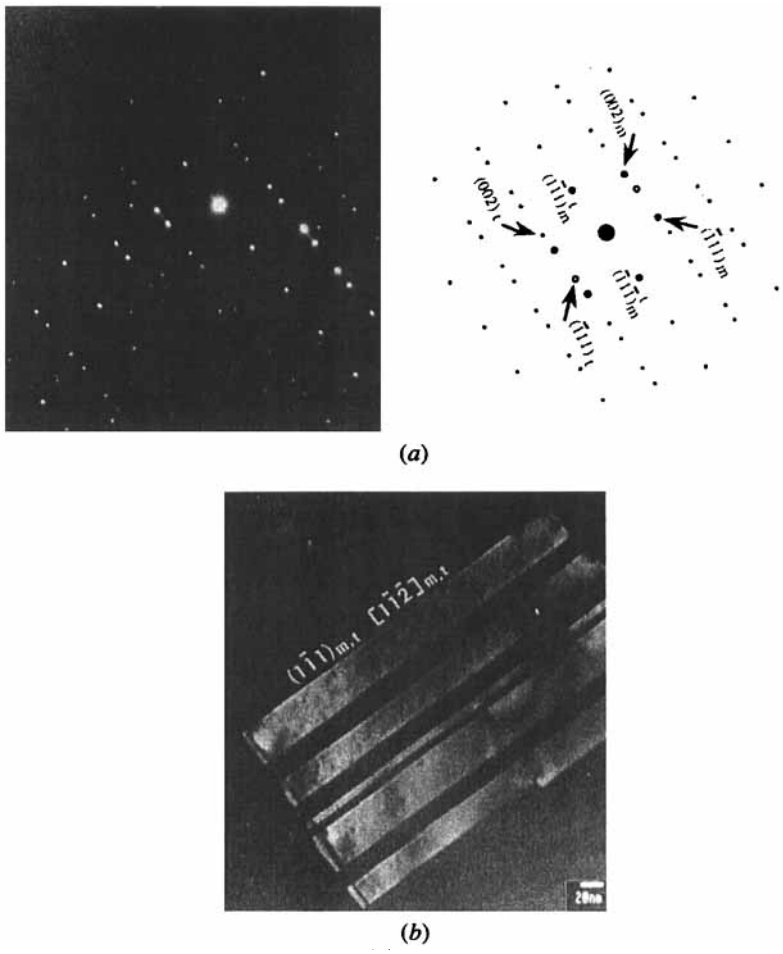

(*a*)

(*b*)

(*a*) ⟨110⟩ SAED pattern from type-1 grain together with its computer-generated simulation for α_1 (m, matrix; t, twin). (*b*) Dark-field (DF) image using twin reflections in fig. 2(*a*).

Type-2 grains revealed the dislocation structure shown in fig. 3. SAED from this grain contains reflections from both the disordered α_1 phase and the ordered $AuCu_3$ phase. Figure 4, which is phase contrast (PC) image from such a grain, shows two unidirectional zones forming a right angle between them, as is expected, bearing in mind the formation of PAPBs on the {001} atomic planes. The unusual angles (not 90°) are shown in fig. 5(*a*) and the corresponding ⟨001⟩ SAED pattern with its computer simulation in fig. 5(*b*). The diffraction pattern also includes the reflections from α_1 epitaxially related to those from $AuCu_3$ II, as expected. The splitting of the superlattice spots is inversely proportional to the domain size, M, i.e. to the distance between two neighbouring PAPBs. According to a given separation, the domain size is approximately $5 < M < 5{\cdot}5$ cells, which is in excellent accordance with the value of 20 Å measured directly from the PAPB images. However, the SAED pattern belongs to the $AuCu_3$ II superlattice, which is supposed to have $M = 9$ cells (when stoichiometric and without additional elements) (Scott 1960). EDS of individual type-2 grains (in scanning transmission electron microscopy (STEM)) in our samples detected about

Fig. 3

Type-2 grain, which is a dislocated $AuCu_3$ II grain.

Fig. 4

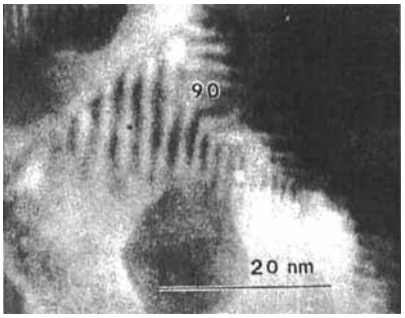

PC image of two unidirectional zones meeting at 90°, as expected.

4–5 at.% Ag in the $AuCu_3$ II phase (Goldfarb *et al.* 1994). It is known (Sato and Toth 1961, 1962, Toth and Sato 1962) that Ag influences the domain size in Au–Cu LPSs. This point will be discussed more extensively in the next section.

Detailed trace analysis of the image in fig. 5 (*a*) (using fig. 5 (*b*)) discovered twinning, which also followed from the streaking of the {100} reflections in the ⟨110⟩ directions (figs 5 (*b*) and 7 (*b*)). According to Hirsch, Howie, Nicholson, Pashley and Whelan (1977) twins on the {111} atomic planes result in the presence of twin points, reducing the spacing between the planes of reciprocal lattice points parallel to (001) by a factor of three, as shown schematically in fig. 6, and in the actual micrographs by Murr (1970).

In fact, absolutely identical SAED patterns were obtained by us from the twin shown in fig. 2 (*b*). Such an ⟨001⟩ SAED pattern is shown in fig. 7 (*a*) and contains twin spots as well as double-diffraction spots (compare with fig. 6). The same features, except for the double-diffraction spots, are clearly seen in the ⟨001⟩ SAED pattern from $AuCu_3$ II LPS in fig. 7 (*b*), which is the magnified pattern of fig. 5 (*b*). Thus, twin spots are close

Fig. 5

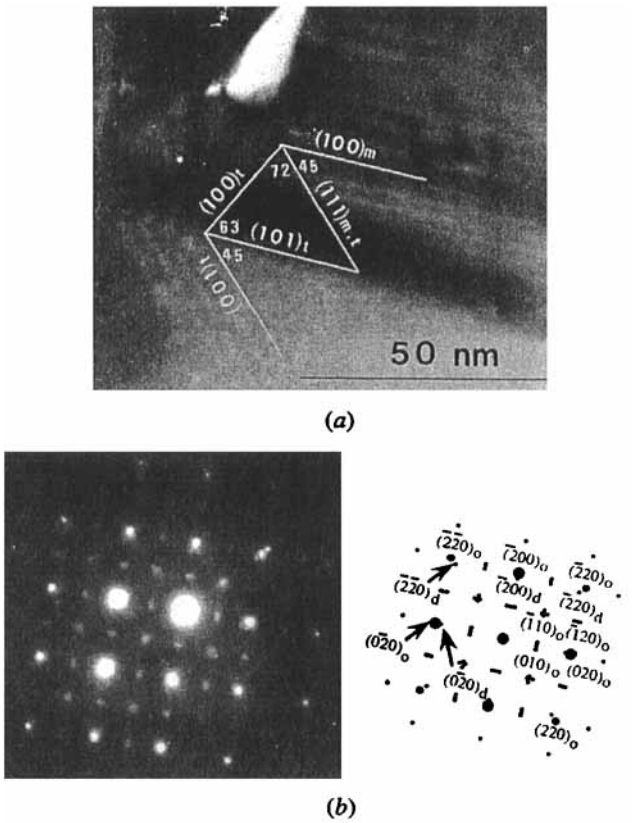

(*a*) DF image showing the parent matrix and the twin, formed using the (110)-matrix and twin spots in fig. 5(*b*). (*b*) ⟨001⟩ SAED pattern from the area in (*a*), and its computer simulation. o, Ordered; d, disordered.

Fig. 6

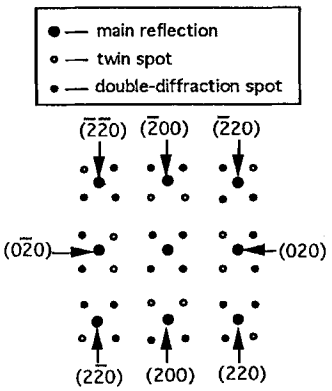

⟨001⟩ SAED pattern revealing {111} twin and the respective double-diffraction spots (from Hirsch *et al.* 1977).

Fig. 7

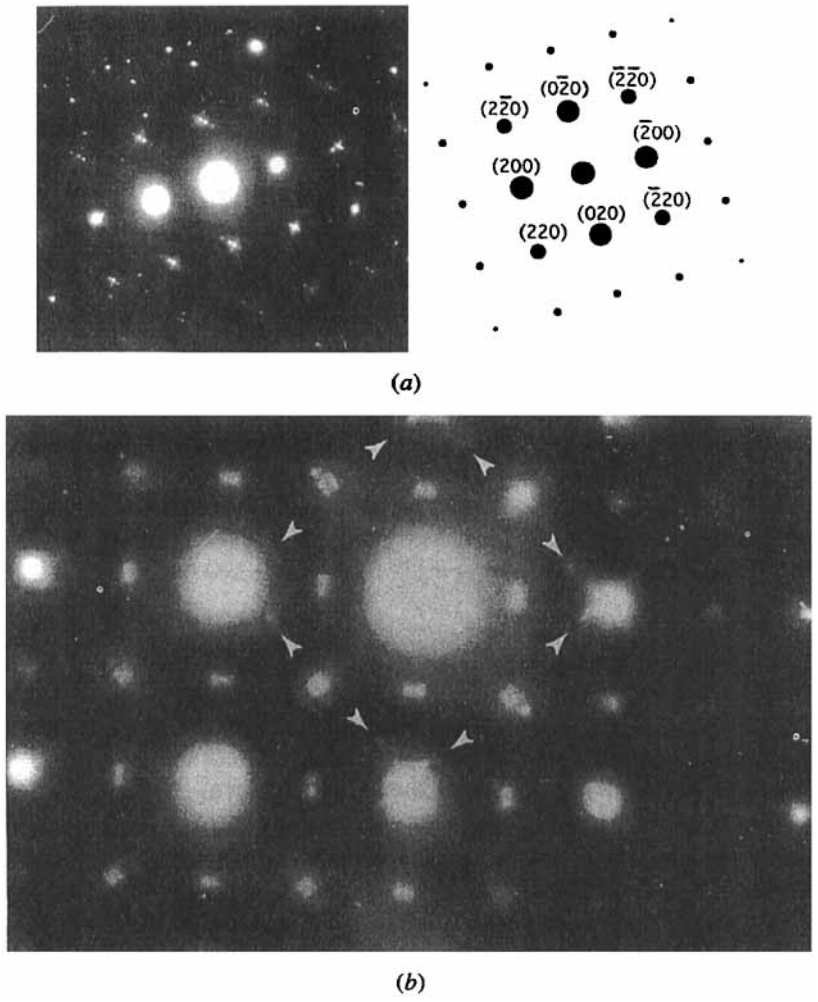

(*a*) ⟨001⟩ SAED pattern from the twinned grain of the α_1 phase. (*b*) Magnified SAED pattern from fig. 5 (*b*). Twin spots are indicated by arrows.

enough to the matrix reciprocal lattice (001) plane, that they contribute to the diffraction pattern and, correspondingly, to the DF image in fig. 5 (*a*).

According to trace analysis, the angles indicated in fig. 5 (*a*) result from the intersection of the planes indicated with the (001) surface, when the parent matrix is oriented with respect to the twin by Kelly's relations (Kelly 1965), i.e.

$$[001]_m \| [221]_t$$

$$(110)_m \| (110)_t$$

as can be easily measured on the superimposed stereographic projection. It follows that the DF image in fig. 5 (*a*) consists of the $(100)_m$ unidirectional zone (of PAPBs), and two unidirectional zones of the twin, $(100)_t$ and $(001)_t$.

A better way to observe the PAPBs is a PC image, and such an image of two unidirectional zones of a twin, viewed along the ⟨001⟩ zone of SAED similar to that

Fig. 8

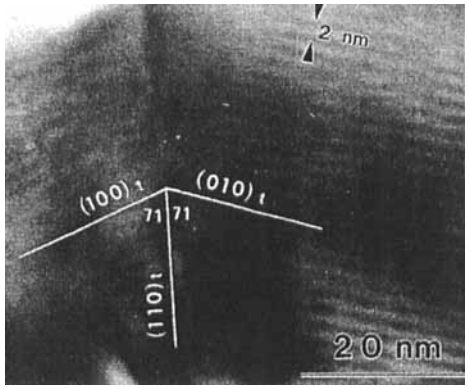

PC image of two unidirectional zones of another twin (matrix is not shown).

of fig. 5 (*b*), is shown in fig. 8 (the matrix is not shown in this figure). Using the same Kelly's projection, the angle of 143° between the unidirectional zones is indicative of $(100)_t$ and $(010)_t$. The distance between the PAPBs is ≈ 20 Å.

§ 4. Discussion

In this section the 'Brillouin zone (BZ), energy lowering mechanism' is proposed as a possible cause for the observed twinning. It is important to stress that twins in ordered systems were observed before, but not in LPSs. For example, Pashley, Robertson and Stowell (1969) and Smith and Bowles (1960) reported that disordered α_1 and ordered AuCu I and AuCu II, respectively, are related by twinning, which is quite well understood as a way to release the strain caused by a tetragonal distortion of AuCu I, or an orthorhombic distortion in the case of AuCu II.

The present case is different, since both the matrix and the twin are the same LPS $AuCu_3$ II phase, and there is no need for strain relief, due to the cubic symmetry of the basic $L1_2$ subcell of $AuCu_3$. The model assumes the formation of twins from superlattice stacking faults rather than from CSF (Paxton 1992). Since the twin energy is roughly half the superlattice fault energy, the proposed BZ-lowering of the SISF energy implies a higher probability for the process of twinning.

In a disordered f.c.c. alloy the introduction of SF does not alter the configuration between the nearest-neighbour atoms, so there is no net change in cohesive energy. In addition, the lattice from both sides of the defect remains unchanged. Thus, neglecting end effects, there is no lattice deformation, but only a packing shift in the $\langle 121 \rangle$ direction. The result is a local discontinuity of the lattice, i.e. the formation of a new surface. It was claimed by Seeger (1965) that the nearer the Fermi surface to the Brillouin zone boundaries, the higher the SF energy, due to electron scattering on the created unperiodicity. However, Seeger's suggestion is not always correct, since there could be a competing mechanism that lowers the electron energy, whenever the Fermi surface touches the zone boundaries (Jones 1934 a, b, 1937). One may also regard SF energy as the free energy difference between f.c.c. and h.c.p. phases (Davies and Cahn 1962, Foley, Cahn and Raynor 1963). This is quite a logical correlation; the more stable the lattice, the harder it is to create SF, as was explicitly shown by the experiments of Hodges (1967). Such an approach is certainly supported by our model. Mikkola and Cohen (1961) suggested the possible effect of the diffused hexagonal zone associated

with SF on the SF energy, which is also supported by our model. The same reasoning is valid to $L1_2$ and $D0_{19}$, $D0_{24}$ ordered structures; the SISF, for example can serve as a criterion for the relative $L1_2$–$D0_{19}$ stability (Paxton 1992).

It was found that in some systems ordering caused an increase in SF energy (for instance Ni_3Mn) but in $AuCu_3$ it caused the reverse effect (Mikkola and Cohen 1961, Marcinkowski and Zwell 1963, Sastry and Ramaswami 1976). In the framework of the currently proposed model this effect reflects the increased interaction between the Fermi surface and the newly formed Jones zone boundaries.

A very similar interaction of the Fermi surface with the boundaries of the Brillouin zone leading to the stability of LPSs is well described in the work of Sato and Toth (1961, 1962, 1963). In a free-electron approximation, the energy of a state with wave vector $\mathbf{k}_i$ equals:

$$E_i = 3{\cdot}79\,|\mathbf{k}_i|^2 \tag{1}$$

and the Fermi energy is expressed as

$$E_F = 36{\cdot}1\{(e/a)/\Omega\}^{2/3}, \tag{2}$$

where Ω is an atomic volume in $Å^3$, e/a is a number of electrons per atom and E_i, E_F are measured in eV when k_i is in $Å^{-1}$. The most primitive cell of the $AuCu_3$ has a basis of four atoms and cubic symmetry and therefore, using eqn. (2), $E_F \approx 6{\cdot}5$ eV. To calculate the energy at the Brillouin zone boundaries one must consider the II-zone, since the I-zone is completely filled and of no importance. The II-zone, which can accommodate 1 electron/atom, is bounded by 12 {110} discontinuity surfaces forming a symmetric rhombic dodecahedron (Sato and Toth 1962), just like the I-zone for b.c.c. The magnitude of a **k**-vector connecting the zone centre to the centre of the discontinuity surface is $\pi 2^{1/2}/a$, and, consequently the electron energy deduced from eqn. (1) is: $E_{\{110\}} \approx 5{\cdot}31$ eV. Since the energy gap on the {110} discontinuity surfaces, $E_g = 0{\cdot}54$ eV, as experimentally measured by Deimel, Higgins and Goodall (1982), is substantially lower than the difference $E_F - E_{\{110\}} = 1{\cdot}2$ eV, overlapping to the next zone occurs. According to Sato and Toth (1961) the degree of overlapping will be reduced (and correspondingly the stability of the structure will be increased) when the split zone boundaries are introduced by LPS formation. In our opinion, a similar mechanism accounts also for the previously mentioned reduction in SF energy. In the framework of the proposed model, the broadening of diffraction patterns, and hence the diffuseness of Brillouin zones, is caused by the intermixing of the hexagonal zones owing to planar defects with the originally cubic zones. In order to demonstrate this concept we shall construct the hexagonal zone and calculate the resultant energy lowering.

4.1. *The SF model*

The SISF shift vector is of the 1/3⟨112⟩-type (Yamaguchi *et al.* 1981). Thus the basis vectors of the hexagonal unit cell formed by SISF in a real lattice will refer to the original cubic cell with the lattice constant a, as follows (see fig. 9): $\mathbf{A}_1 = (a/2)[\bar{1}10]$; $\mathbf{A}_2 = (a/2)[0\bar{1}1]$; $\mathbf{A}_3 = (2a/3)[111]$. The angle between $\mathbf{A}_1$ and $\mathbf{A}_2$ is 120°, and the magnitude of $\mathbf{A}_3$ is two d-spacings in the ⟨111⟩ direction. The volume of such a hexagonal cell is half that of the original cubic cell ($V_h = a^3/2$), but contains only two atoms, which leaves the same atomic volume. The reciprocal lattice basis vectors are; $\mathbf{B}_1 = (2\pi/a)[\bar{4}/3\ 2/3\ 2/3]$; $\mathbf{B}_2 = (2\pi/a)[\bar{2}/3\ \bar{2}/3\ 4/3]$; $\mathbf{B}_3 = (2\pi/a)[1/2\ 1/2\ 1/2]$, and the volume of the Brillouin zone is: $V_B = 2(2\pi/a)^3$. However, the actual I-zone is a truncated

Fig. 9

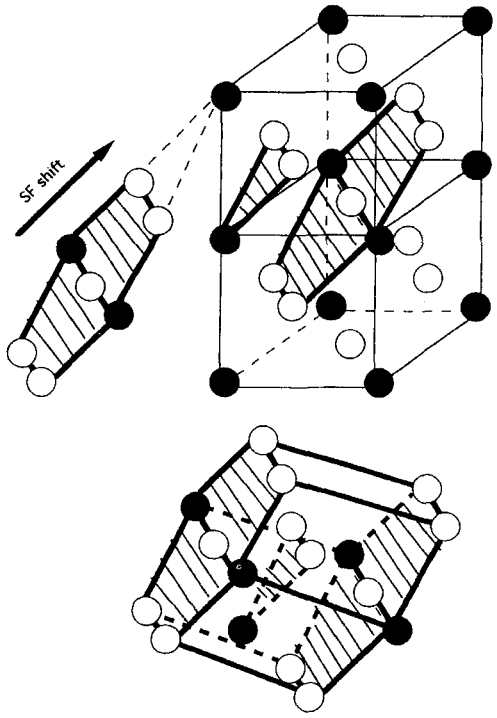

Hexagonal cell created by SISF operation. Open circles denote Cu atoms.

Fig. 10

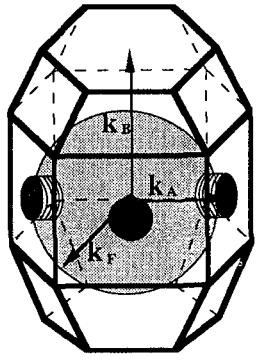

Configuration of the Fermi surface in the hexagonal Jones zone formed by SF.

II-zone, since there are no energy discontinuities on the basal hexagonal {0001} faces. Thus the real zone is the so-called 'Jones zone' (fig. 10) with a volume of $V_J \approx 1{\cdot}75V_B$, and in the case of an ideal axial ratio of 1·633, it can accommodate 1·75 electrons/atom (Altmann 1970). The Fermi energy remains the same as for a cubic zone, but the wave vectors to the zone boundaries are now given by

$$|\mathbf{k}_A| = \pi 2^{3/2}/(3^{1/2}a) \text{ and } |\mathbf{k}_B| = \pi 3^{1/2}/a \tag{3}$$

where subscript A designates the prismatic planes and B the basal planes (see fig. 10).

One can calculate the electron energies using expressions (1) and (3) with $a = 3{\cdot}75$ Å for $AuCu_3$. The results are: $E_A \approx 7{\cdot}1$ eV and $E_B \approx 8{\cdot}0$ eV. Since $E_F \approx 6{\cdot}5$ eV, the stabilization will take place on the A faces. The closest boundaries (A) will now be at some distance away from the Fermi surface, compared to the situation before the creation of the SF. The crystal is now subjected to a shear, which changes the atomic configuration without changing the volume, and the result is a movement of Brillouin zone boundaries. Owing to the volume invariance, the density of states in the reciprocal lattice remains unchanged, as in the Fermi surface, which now close to, but not touching the discontinuity surfaces.

This case resembles that analysed by Goodenough (1952). He claimed that in such an instance the Fermi surface will exert an attractive force on the closest boundaries in order to have them in contact. When such a contact is established, there will be a lowering of the average electron energy, and in the contact area the lowering is roughly $E_g/2$ (Altmann 1970). The more precise calculations should take into account the modification of the density of states near the zone boundary and the volume in reciprocal space where the electron spectrum is actually changed. This procedure is rather complicated, because the detailed spectrum of the electron states in $AuCu_3$ is unknown. Nevertheless, some estimations can be made. The lowering of the average electron energy is expressed as:

$$\Delta E = -(1/2)\langle E \rangle = -(3/5)(E_F/2). \tag{4}$$

However, the modification of the spectrum affects only some small volume, V_a, inside the Brillouin zone, which is, in fact, a 'neck' volume. Taking a cylindrical shape for a 'neck' in the Jones zone for $AuCu_3$, with radius $r = k_f/7$ and height $\Delta k = |\mathbf{k}_A| - |\mathbf{k}_F| = 0{\cdot}045 k_F$, one obtains the required ratio, η, of V_a to the volume of Fermi sphere (see fig. 10):

$$\eta = V_a/V_F = 7 \times 10^{-4}. \tag{5}$$

Now, the final gain, γ_{BZ}, of the electron energy is found as the product:

$$\begin{aligned} \gamma_{BZ} &= -6\eta\, \Delta E = -8{\cdot}25 \times 10^{-3}\,\text{eV/electron} \\ &= -8{\cdot}25 \times 10^{-3}\,\text{eV/atom} \approx -22\,\text{mJ m}^{-2} \end{aligned} \tag{6}$$

The factor of 6 in expression (6) reflects the number of equivalent {110} discontinuity surfaces in the Jones zone. γ_{BZ} can explain the differences between the calculated values of the SISF energy (Paxton 1992) and the experimentally measured ones (Marcinkowski 1963, Sastry and Ramaswami 1976), although it cannot account for the magnitude of these differences.

It is known that even in pure f.c.c. noble metals the Fermi surface slightly deviates from the spherical shape due to 'neck' formation in the vicinity of the {111} discontinuity surfaces (Morse 1960). The radius of the 'neck' connecting the Fermi surface to the nearest boundary in noble metals decreases in the following order: Cu → Au → Ag (Mikkola and Cohen 1961), and so does the SF energy (Vassamillet and Massalski 1963). Therefore, the probability of the SF formation increases in that order.

The origin of the 'intrinsic' SF energy (as in pure metals) may be assessed in the light of this concept of 'neck' radius. When the 'neck' radius (and the contact area) is small, the average electron energy is lowered, and such a configuration will be a favourable one. When the Fermi surface starts to intersect the boundary of the energetic discontinuity, it pulls the boundary towards the zone centre, increasing the overlap until

the electrons can 'spill-out' into the next zone. With the formation of SISF, 'neck' radii in $AuCu_3$ are reduced, decreasing the electron energy and thus stabilizing the defect.

Furthermore, as was previously mentioned, our EDS results in STEM indicated the presence of 4–5 at.% of Ag in $AuCu_3$ II phase (Goldfarb *et al.* 1994). It is known (Vassamillet and Massalski 1963) that dissolved Ag even at concentrations of a few atomic per cent lowers the SF energy in pure Cu and Au by factor $\xi \approx 4$. It was also experimentally shown that the 'neck' radius of the $AuCu_3$ is actually a weighted average of the Au and the Cu 'neck' radii (Deimel *et al.* 1982), implying the similar reduction of the SISF energy in the $AuCu_3$(Ag) alloy.

It is important to stress the significance of silver in the process of SISF and, correspondingly, twin stabilization: taking the SISF energy as $120\,mJ\,m^{-2}$ (Paxton 1992), the energy lowering due to γ_{BZ} is only 17% in the case of a binary $AuCu_3$ alloy. However, in the ternary $AuCu_3$(Ag) alloy, assuming the same reduction factor $\xi \approx 4$ as in pure metals, the actual energy may be lower by 73%, implying twin concentration substantially higher than in a binary $AuCu_3$ alloy!

4.2. *Additional applications of the SF model*

In this section, using the proposed model, we can also offer a plausible explanation for the composition effect (when *e/a* is unchanged) on *M*, which remained unclear from the Sato and Toth theory. In their model the domain size of LPS is determined by the following expression (Sato and Toth 1961, 1962) and depends only on *e/a* and the topology of the Fermi surface:

$$e/a = [\pi/(12t^3)]\{2 \pm 1/M + 1/4M^3\}^{3/2}, \tag{7}$$

where t is the truncation factor, which defines the deviation of the Fermi surface from a spherical shape. The ($\pm$) sign reflects the possibility of stabilization on the split inner ($-$) or outer ($+$) Brillouin zone boundaries. In the case of $AuCu_3$ II the stabilization takes place on the outer boundaries, due to the relatively large size of the Fermi surface. It is clear from eqn. (7) that the only way to vary M at constant *e/a* is by changing t. However, the specific mechanism of t-modification has not been suggested. In our opinion this mechanism is also related to the probability of SF in LPS.

The domain size of $AuCu_3$ II in our samples containing 4–5 at.% Ag was measured as 20 Å, which is approximately 5 subcells. Such a domain size corresponds to $t \approx 0{\cdot}95$, according to eqn. (7). Following the measurements of Scott (1960), the domain size of $AuCu_3$ II containing no Ag is ≈ 9 cells, which corresponds to $t \approx 0{\cdot}92$. Thus, the higher value of t in our samples may be associated with the effect of dissolved Ag on SF energy, as will be demonstrated below. On the same basis we can analyse some experimental results obtained by other investigators. For example, Toth and Sato (1962) observed a decrease in the domain size of $AuCu_3$ II with the addition of Au, which implies the opposite effect for Cu addition. Therefore both Ag and Au diminish the domain size in $AuCu_3$ II LPS, contrary to the influence of Cu. That is why one can exclude, for example, the difference in the effective valences between Au, Ag and Cu as a possible cause for the M variation. Au and Cu have a very similar electronic band structure, as might be deduced from various optical measurements, differing from the electronic structure of Ag which reflects light outside the visual spectrum. Thus the effective valence difference would cause the opposite effect to that observed. On the other hand, the atomic sizes of Au and Ag are very close to each other, differing considerably from the atomic size of Cu.

The more quantitative explanation of these tendencies in the framework of our

Solid solution effects of Au, Ag and Cu dissolved in Au, Ag and Cu.

Solute	Atomic volume	Atomic size factors (%)			Effective volumes (Å^3)		
	Ω (Å^3)	Ω_s^{Au}	Ω_s^{Ag}	Ω_s^{Cu}	$\Omega_{eff.}^{Au}$	$\Omega_{eff.}^{Ag}$	$\Omega_{eff.}^{Cu}$
Au	16·96	—	− 1·0	+ 47·9	—	16·89	17·47
Ag	17·06	− 0·5	—	+ 40·8	16·88	—	16·63
Cu	11·81	− 14·2	− 26·9	—	14·55	12·47	—

Fig. 11

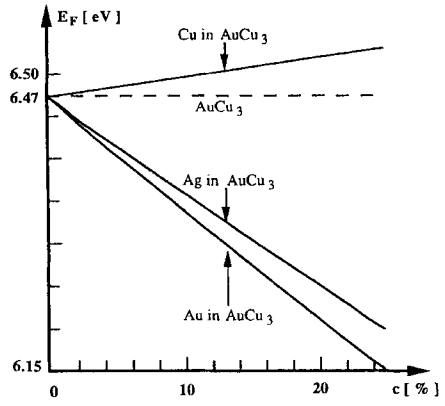

Dependence of the $AuCu_3$ II Fermi energy on the additions of Au, Ag and Cu.

model requires the use of the 'atomic size factor', Ω_s. According to King (1963), when an atom *B* is dissolved in the atomic matrix of A, its effective atomic volume is changed from Ω_B to Ω_{eff} owing to modification of atomic bonding. The solution of B atoms in the matrix of A also leads to a variation in the average volume per atom in the solution. This variation is defined as Ω_s:

$$\Omega_s = (\Omega_{eff} - \Omega_A)/\Omega_A. \tag{8}$$

Knowing the atomic size factors for Au, Ag and Cu when dissolved in Au, Ag and Cu, one can calculate their effective atomic volumes in these solutions. The atomic volumes of Au, Ag and Cu, their size factors when dissolved in Au, Ag and Cu, and their effective atomic volumes (Ω_{eff}) calculated from eqn. (8), are given in the table. Knowing these effective volumes it is possible to calculate the average volume per atom in $AuCu_3$, depending on the concentration, *c*, of the Au, Ag and Cu solutes, using the following expressions:

$$\Omega_{AuCu_3} = (1 - c)13{\cdot}18\,\text{Å}^3 + c(16{\cdot}88\,\text{Å}^3 \times 0{\cdot}25 + 16{\cdot}63\,\text{Å}^3 \times 0{\cdot}75) \tag{9}$$

for dissolved Ag,

$$\Omega_{AuCu_3} = (1 - c)13{\cdot}18\,\text{Å}^3 + c(17{\cdot}47\,\text{Å}^3 \times 0{\cdot}25 + 16{\cdot}96\,\text{Å}^3 \times 0{\cdot}75) \tag{10}$$

for dissolved Au, and

$$\Omega_{AuCu_3} = (1 - c)\ 13{\cdot}18\,\text{Å}^3 + c(14{\cdot}55\,\text{Å}^3 \times 0{\cdot}25 + 11{\cdot}81\,\text{Å}^3 \times 0{\cdot}75) \tag{11}$$

for dissolved Cu. The value of 13·18 Å^3 is the initial atomic volume for the stoichiometric $AuCu_3$. The definitions (9)–(11) for the average Ω_{AuCu_3} in non-stoichio-

metric alloys reflect the probability that the solute atom is bonded to Au or Cu neighbours. Generally, expressions like eqns (9)–(11) are correct for dilute solutions. However, in many cases such linear dependencies (Veggard rule) can be applied for rather large concentrations. For example, in our case the measured atomic volume of $AuCu_3$ is precisely equal to

$$\Omega_{AuCu_3} = 13{\cdot}18\,\text{Å}^3 = \Omega_{Au} \times 0{\cdot}25 + \Omega_{Cu} \times 0{\cdot}75. \tag{12}$$

(Note that the same linear dependence describes the behaviour of the 'neck' radius in $AuCu_3$, implying the correlation outlined in our model!). Substituting Ω_{AuCu_3} from the expressions (9)–(11) into eqn. (2), we can calculate the variation of the Fermi energy, E_F, with composition. The dependence of E_F for $AuCu_3$ on the concentrations of Au, Ag and Cu is shown in fig. 11. It is obvious now that when both Ag or Au are added to $AuCu_3$, they lower the E_F, while the addition of Cu increases the E_F. The Fermi energy (E_F), 'neck' radius and SISF energy vary in the same direction, and inversely to the variation of the truncation factor, t.

Thus it may be concluded that the addition of Au or Ag to $AuCu_3$ will lead to a higher average truncation factor (resulting from the increased number of Jones zones) and, consequently, to smaller domain size, M, according to expression (7). The reverse effect caused by Cu addition is obvious from the same considerations. There are, perhaps, various other plausible explanations for the M variations when e/a is constant, based on short-range atomic interactions, temperature dependence, etc. In general, M is determined by the balance between long-range Fermi surface effects and the short-range chemical interactions, which is why not all alloys display LPS behaviour. However, the role of short-range interactions is important mostly in regular ordered phases, contrary to the systems where LPSs are actually formed (Sato and Toth 1961). The results of Sato and Toth explicitly demonstrate the dependence of M almost solely upon electron concentration (long-range interactions). Tachiki performed most detailed quantitative calculations including the effects of repulsive interaction between ion cores, the interaction with conduction electrons, and even the elastic energy effect (in the case of AuCu I, II) and yet their final conclusions were identical to Sato and Toth's model (Tachiki and Teramoto 1966). They claimed that in the case of noble metal alloys based on the f.c.c. lattice, the repulsive energy plays no role in the determination of M. Similar results were obtained for Cu–Pt and Cu–Pd (Kubo and Adachi 1973) systems, as well as for several other systems (Tachiki and Maekawa 1970). The most recent work in the Ag–Mg system confirms that the LPS stabilization is achieved by the presence of superlattice zone boundaries at parallel regions of the Fermi surface, when the basic cell is $L1_2$ (Jordan *et al.* 1993).

All these findings show convincingly that the main driving force in LPS stabilization is the topology of the Fermi surface. As a result of the appearance of charge density waves (CDWs), the variations of the LPS period (M) with composition are determined by configuration of Fermi surfaces relative to Brillouin zone boundaries and still obey the same basic equation (7) as derived by Sato and Toth. As for the temperature dependence of M as a possible reason for M variation from $M = 9$ to $M = 5$, it was shown by recent computer modelling (Koyama and Ishimaru 1990, Koyama and Mori 1991) using a Ginsburg–Landau free-energy functional, that M increases with decreasing temperature, and the degree of change is larger the longer the period. In real systems, the Cu–Pd behaviour (Takeda, Kulik and de Fontaine 1988) is close to the calculated behaviour, but only slight temperature dependence was recorded in the Au–Cu system, which could not account for such a large M difference.

§ 5. Conclusions

Series of samples containing Au–Ag–Cu alloys with continuously varied compositions were obtained by subsequent magnetron sputtering of thin Au, Ag and Cu films, followed by heat treatments. Prior to heat treatments almost no interdiffusion between the layers occurred. In fact, XRD measurements of the untreated samples indicated the formation of artificially composition-modulated superstructures in the direction perpendicular to the film surface.

The annealed samples revealed phases formed in general accordance with the Au–Ag–Cu phase diagram, as was evident from XRD, EDS and TEM studies. Long-period superlattice $AuCu_3$ II was found among these phases. The microstructure of this LPS contains numerous defects, such as dislocations, SF and, observed for the first time, twins.

In order to explain the twin formation in LPS a model has been proposed, based on the electron theory of metals. According to this model, SISF create hexagonal Jones zones in the reciprocal lattice. Interaction between the Fermi surfaces and the boundaries of Jones zones fosters the stabilization of twins by means of the reduction of electron energy. Such a stabilization is even more enhanced in ternary $AuCu_3(Ag)$ II, as was demonstrated by numerical estimates of the γ_{BZ} contribution to SISF energy and, consequently increases the probability for twin growth.

The essence of the proposed model is the correlation between the Fermi energy, the radius of the 'neck' formed at the contact with zone boundaries, the SISF energy and the truncation factor, t. The last quantity directly determines the domain size, M, with a given electron density, e/a. The established correlation allows qualitative explanation of the observed influence of Au, Ag and Cu concentration on the domain size of $AuCu_3$ II.

The basis of our model is the theory of Sato and Toth. Although more complicated and advanced LPS theories, such as CDWs, etc., have been developed since then, detailed analysis shows that in principle the simple and visual ideas of Sato and Toth can nevertheless be used for physical estimations. Recent publications (Dimiduk, Rao, Parthasarathy and Woodward 1992, Hemker and Mills 1993) indicate that the stabilization mechanism proposed by us may also play an important role in the stabilization of ordinary (not LPS) ordered structures, such as Ni_3Al, relative to the disordered state, but in this case short-range interactions are also certainly important.

Acknowledgments

The authors wish to express their gratitude to Professor D. Shechtman for fruitful discussions. His help is gratefully acknowledged.

References

Altmann, S. L., 1970, *Band Theory of Metals* (Oxford: Pergamon).

Barret, C. S., and Massalski, T. B., 1980, *Structure of Metals* (Oxford: Pergamon).

Davies, R. G., and Cahn, R. W., 1962, *Acta Metall.*, **10,** 621.

Deimel, P. P., Higgins, R. J., and Goodall, R. K., 1982, *Phys. Rev.* B, **24,** 6197.

Dimiduk, D. M., Rao, S., Parthasarathy, T. A., and Woodward, C., 1992, *Ordered Intermetallics—Physical Metallurgy and Mechanical Behavior*, edited by C. T. Liu *et al.* (Dordrecht: Kluwer).

Flinn, P. A., 1958, *Trans. AIME*, **218,** 145.

Foley, J. H., Cahn, R. W., and Raynor, G. W., 1963, *Acta Metall.*, **11,** 355.

Glossop, A. B., and Pashley, D. W., 1959, *Proc. roy. Soc.* A, **250,** 132.

Goldfarb, I., Zolotoyabko, E., and Shechtman, D., 1993a, *Mater. Res. Symp. Proc.*, **311,** 39; 1993b, *J. appl. Phys.*, **74,** 2501.

GOLDFARB, I., ZOLOTOYABKO, E., BERNER, A., and SHECHTMAN, D., 1994, *Mater. Lett.*, **21,** 149.
GOODENOUGH, J. B., 1952, *Phys. Rev.*, **89,** 282.
GYORFFY, B. L., and STOCKS, G. M., 1983, *Phys. Rev. Lett.*, **50,** 374.
HEMKER, K. J., and MILLS, M. J., 1993, *Phil. Mag.* A, **68,** 305.
HIRSCH, P., HOWIE, A., NICHOLSON, R. B., PASHLEY, D. W., and WHELAN, M. J., 1977, *Electron Microscopy of Thin Crystals* (Florida: Robert E. Krieger).
HODGES, C. H., 1967, *Phil. Mag.*, **15,** 371.
JONES, H., 1934a, *Proc. roy. Soc.* A, **144,** 225; 1934b, *Ibid.*, **147,** 396; 1937, *Proc. Phys. Soc.*, **49,** 250.
JORDAN, R. G., YAN LIU, QIU, S. L., XUMOU XU, DURHAM, P. J., and GUO, G. Y., 1993, *Phys. Rev.* B, **47,** 16521.
KELLY, P. M., 1965, *Trans. AIME*, **233,** 264.
KING, H. W., 1963, *Alloying Behavior and Effects in Concentrated Solid Solutions*, Vol. 29, edited by T. B. Massalski (New York: Gordon and Breach, Metallurgical Society Conferences).
KOYAMA, Y., and ISHIMARU, M., 1990, *Phys. Rev* B, **41,** 5378.
KOYAMA, Y., and MORI, S., 1991, *Phys. Rev.* B, **44,** 8522.
KUBO, S., and ADACHI, K., 1973, *J. Phys. Soc. Jap.*, **35,** 776.
MARCINKOWSKI, M. J., 1963, *Electron Microscopy and Strength of Crystals*, edited by G. Thomas and J. Washburn (New York: Inter-Science).
MARCINKOWSKI, M. J., and ZWELL, L., 1963, *Acta metall.*, **11,** 373.
MENON, E. S. K., HUANG, P., KRAITCHMAN, M., HOYT, J. J., CHOW, P., and DE FONTAINE, D., 1992, *Mater. Res. Soc. Symp. Proc.*, **205,** 137.
MIKKOLA, D. E., and COHEN, J. B., 1961, *J. appl. Phys.*, **33,** 892.
MORSE, R. W., 1960, *International Conference on the Fermi surface* (New York: Wiley).
MURR, L. E., 1970, *Electron Optical Applications in Material Science* (New York: McGraw-Hill).
NAKAGAWA, M., and YASUDA, K., 1988, *J. less-common metals*, **138,** 95.
OGAWA, S., 1974, *Order–Disorder Transformations in Alloys*, edited by H. Warlimont (Berlin: Springer-Verlag).
PASHLEY, D. W., and PRESLAND, A. E. B., 1959, *J. Inst. Metall.*, **87,** 419.
PASHLEY, D. W., ROBERTSON, J. L., and STOWELL, M. J., 1969, *Phil. Mag.*, **19,** 83.
PAXTON, A. T., 1992, *Electron Theory in Alloy Design*, edited by D. G. Pettifor and A. H. Cottrell (London: The Institute of Materials).
PRINCE, A., 1988, *Int. Mater. Rev.*, **33,** 314.
SASTRY, S. M. L., and RAMASWAMI, B., *Phil. Mag.*, **33,** 375.
SATO, H., and TOTH, R. S., 1961, *Phys. Rev.*, **124,** 1833; 1962, *Phys. Rev.*, **127,** 469; 1963, *Alloying Behaviour and Effects in Concentrated Solid Solutions*, Vol. 29, edited by T. B. Massalski (New York: Gordon and Breach, Metallurgical Society Conferences).
SCOTT, R. E., 1960, *J. appl. Phys.*, **31,** 2112.
SEEGER, A., 1965, *Dislocations and Mechanical Properties of Crystals*, edited by J. C. Fisher, W. G. Johnson, R. Thomson and T. Vreeland (New York: Wiley).
SHECHTMAN, D., BLACKBURN, M. J., and LIPSITT, H. A., 1974, *Trans. Met.*, **5,** 1373.
SMITH, R., and BOWLES, J., 1960, *Acta Metall.*, **8,** 405.
STOCKS, G. M., NICHOLSON, D. M., PINSKI, F. J., BUTLER, W. H., STERNE, P., TEMMERMAN, W. M., GYORFFY, B. L., JOHNSON, D. D., GONIS, A., ZHANG, X. G., and TURCHI, P. E. A., 1987, *Mater. Res. Soc. Symp. Proc.*, **81,** 15.
TACHIKI, M., and MAEKAWA, S., 1970, *J. Phys. Soc. Jap.*, **28,** 375.
TACHIKI, M., and TERAMOTO, K., 1966, *J. Phys. Chem. Solids*, **27,** 335.
TAKEDA, M., and HASHIMOTO, H., 1985, *Phys. Stat. sol.*, **87,** 141.
TAKEDA, S., KULIK, J., and DE FONTAINE, D., 1987, *Acta metall.*, **35,** 2243; 1988, *J. Phys.* F, **18,** 1387.
TOTH, R. S., and SATO, H., 1962, *J. appl. Phys.*, **33,** 3250.
VASSAMILLET, L. F., and MASSALSKI, T. B., 1963, *J. appl. Phys.*, **34,** 3402.
YAMAGUCHI, M., VITEK, V., and POPE, D. P., 1981, *Phil. Mag.* A, **43,** 1027.
YASUDA, K., 1987, *Gold. Bull.*, **20,** 90.